


Broken Luttinger theorem in the two-dimensional Fermi-Hubbard modelIan Osborne,¹ Thereza Paiva,² and Nandini Trivedi¹¹*Department of Physics, The Ohio State University, Columbus, Ohio 43210, USA*²*Instituto de Física, Universidade Federal do Rio de Janeiro, Caixa Postal 68.528, 21941-972 Rio de Janeiro, Rio de Janeiro, Brazil* (Received 3 June 2020; revised 30 October 2021; accepted 2 November 2021; published 10 December 2021)

One of the fundamental questions about high-temperature cuprate superconductors is the size of the Fermi surface underlying the superconducting state. By analyzing the single-particle spectral function for the Fermi-Hubbard model as a function of repulsion U and chemical potential μ , we find that the Fermi surface in the normal state undergoes a transition from a large Fermi surface matching the Luttinger volume as expected in a Fermi liquid, to a Fermi surface that encloses fewer electrons that we dub the “Luttinger breaking” phase, as the Mott insulator is approached. This transition into a non-Fermi-liquid phase that violates the Luttinger count occurs at a critical density in the absence of any other broken symmetry. We obtain the Fermi-surface contour from the spectral weight $A_{\mathbf{k}}(\omega = 0)$ and from an analysis of the singularities of the Green’s function $\text{Re } G_{\mathbf{k}}(E = 0)$, calculated using determinantal quantum Monte Carlo and analytic continuation methods. We discuss our numerical results in connection with experiments on Hall measurements, scanning tunneling spectroscopy, and angle-resolved photoemission spectroscopy.

DOI: [10.1103/PhysRevB.104.235122](https://doi.org/10.1103/PhysRevB.104.235122)**I. INTRODUCTION**

A question of fundamental importance for strongly correlated metals near a Mott transition is, What is the size of the Fermi surface (FS)? Does it count all the electrons or only the carriers relative to the Mott filling? In other words, is the Fermi surface large or small [1]? And furthermore, if the FS deviates from the Luttinger volume, is it due to reconstruction of the FS due to competing order or due to topological order?

We are motivated by three sets of experiments on the cuprates: the Hall coefficient which gives information on the density and type of carriers [2,3], scanning tunneling spectroscopy [4–6] that gives information about broken charge density and pair density order, and angle-resolved photoemission spectroscopy [7–10] that gives information about the momentum-resolved density of states. The Hall number n_H in $\text{YBa}_2\text{Cu}_3\text{O}_y$ (YBCO) shows a distinct change at a critical doping p_c^H from $n_H \approx 1 + p$ at high doping p of holes to $n_H \approx p$ for low doping [2]. The next question is whether the change in behavior of the Hall coefficient occurs due to broken symmetry in the charge, spin, or pairing channels. Scanning tunneling spectroscopy experiments indicate that charge order is observed in YBCO below a critical doping $p_c^{\text{CDW}} < p_c^H$ [4–6,11], which suggests that the mechanism causing the change of the Hall coefficient and the mechanism driving charge order are distinct phenomena.

Here we sharpen the question for the celebrated Hubbard model rather than focusing on analysis of experiments, the latter being undoubtedly more complicated. Early quantum Monte Carlo (QMC) calculations of the spectral function related antiferromagnetic fluctuations to pseudogap formation and quasiparticle weight transfer [12–15]. More recent work focused on systems with particle-hole asymmetry, introduced by next-nearest-neighbor hopping. Cluster dynamical mean-field theory (CDMFT) studies have shown that the

quasiparticles show momentum-dependent renormalizations due to proximity to the Mott transition, even in the absence of long-ranged antiferromagnetic correlations [16–21].

In this paper, our aim is to extract the underlying FS as a function of doping, with particular emphasis on the region close to the Mott transition [22]. We focus on the particle-hole symmetric Hubbard model with only nearest-neighbor hopping. Our main result is that the FS volume follows the Luttinger volume for high densities, but starts deviating below a critical density n_c , as the Mott density is approached (Fig. 1). In other words, the Luttinger-breaking FS does not change abruptly from a volume that counts $(1 + p)$ holes to p holes, but evolves continuously below n_c . A similar evolution occurs on the hole-doped side as well, by particle-hole symmetry for the case studied here with zero next-nearest-neighbor hopping. We also discuss the behavior of $\text{Re } G$ [Eq. (4)] which shows sign changes as the Mott insulator is approached [23,24].

This evolution from a large FS to a small FS is observed in Hall coefficient of single-layer cuprates such as $\text{Ti}_2\text{Ba}_2\text{CuO}_{6+\delta}$ and $\text{Bi}_2\text{Sr}_2\text{CuO}_{6+\delta}$ and is cited as evidence for a “hidden” order that may be responsible for the pairing mechanism of high- T_c superconductors [3,25]. Such ideas have also been discussed in the literature previously [15,16,24,26,27]. The significance of the quantum Monte Carlo simulation results presented here are the insights obtained from the momentum space contour of the spectral function at $\omega = 0$ for a model instead of a material that allows us to interpret features in the spectral function solely to Mott physics. Furthermore, the availability of QMC data on larger lattices allows us to obtain the spectral function on the FS contour on a finer mesh of k points to observe the violation of the Luttinger count close to the Mott transition. The use of four different approaches to obtain the Fermi-surface volume strengthens our findings.

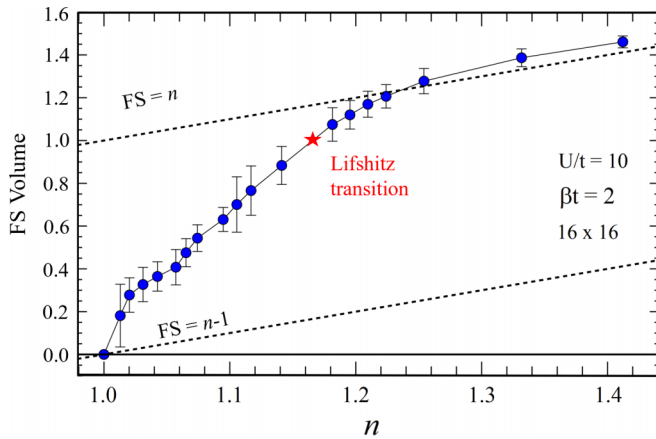


FIG. 1. Evidence for Luttinger-breaking Fermi surface: The Fermi-surface volume deviates strongly from the expected Luttinger volume which is proportional to the charge carrier density, below a critical density n_c as the Mott insulator at $n = 1$ is approached. Determinantal QMC results for the Hubbard model on a 16×16 square lattice for $U/t = 10t$ and $\beta t = 2$ showing $n_c \approx 1.2$.

We calculate the FS contour by using determinantal quantum Monte Carlo methods to obtain the imaginary-time Green's function, $G_{\mathbf{k}}(\tau)$, as a function of the interaction strength, carrier concentration, and temperature. Analytic continuation of G yields the spectral function $A_{\mathbf{k}}(\omega)$ [28–33] whose contour at $\omega = 0$ then yields the FS.

We also analyze the behavior of the Green's function, $\text{Re } G_{\mathbf{k}}(E)$, and find that it changes sign at zero chemical potential in two distinct ways: (i) For densities away from unity, the sign change occurs through a pole, as expected for a system with well-defined quasiparticles [16]. (ii) As the Mott density is approached, the sign change occurs through a zero. Such a behavior was first pointed out by Dzyaloshinskii [23] as occurring in a Mott insulator. In this paper, we find remarkably that the breakdown of the Luttinger count happens in the metallic state approaching the Mott insulator. We show that proximity to a Mott insulator naturally fractionalizes the spectral function into an incoherent lump and a sharper quasiparticle piece, and furthermore the contour in momentum space at zero energy violates the Luttinger count. Notably, the reorganization of states is found to occur in the absence of any competing order, indicating the emergence of a ‘‘Luttinger breaking’’ (LB) non-Fermi-liquid phase.

II. MODELS AND METHODS

The Fermi-Hubbard model is the paradigmatic model for Mott insulators, strongly correlated metals, and high-temperature superconductors. In its particle-hole symmetric form, the Hamiltonian is given by

$$\mathcal{H} = -t \sum_{(i,j),\sigma} (\hat{c}_{i,\sigma}^\dagger \hat{c}_{j,\sigma} + \text{H.c.}) + U \sum_i \left(\hat{n}_{i\uparrow} - \frac{1}{2} \right) \left(\hat{n}_{i\downarrow} - \frac{1}{2} \right) - \mu \hat{N}, \quad (1)$$

defined so that when the chemical potential $\mu = 0$, the average density is unity ensuring that the system is half filled. Here

t is the tunneling amplitude for a fermion to hop from one site to a neighbor without changing the spin, $\sigma = \uparrow, \downarrow$, and U is the on-site Coulomb repulsion. The spatial index i labels a site on a 2D square lattice, and $\hat{c}_{i,\sigma}$ and $\hat{c}_{i,\sigma}^\dagger$ are fermionic annihilation and creation operators, respectively. The number operator is defined as $\hat{n}_{i,\sigma} \equiv \hat{c}_{i,\sigma}^\dagger \hat{c}_{i,\sigma}$, $\hat{n}_i = \hat{n}_{i,\uparrow} + \hat{n}_{i,\downarrow}$, and the particle density per site $n = \sum_i \langle \hat{n}_i \rangle / N_s$, where N_s is the total number of sites. Relative to the filled band with two electrons per site, the hole density is $1 + p$. Particle-hole symmetry is exhibited by the transformation of particle creation and annihilation operators for hole annihilation and creation operators, respectively: $c_{\sigma i}^\dagger \rightarrow (-1)^i d_{\sigma i}$, $c_{\sigma i} \rightarrow (-1)^i d_{\sigma i}^\dagger$. A finite next-nearest-neighbor hopping term, t' , which we do not include in our discussion here, would break particle-hole symmetry in Eq. (1). We calculate thermodynamic properties and the single-particle Green's function by implementing the determinantal QMC algorithm.

III. OBTAINING THE FERMI-SURFACE CONTOUR

Luttinger's theorem asserts that the volume enclosed by the Fermi surface of an interacting Fermi liquid is proportional to the number of particles in the system [1]. This allows us to find the reference noninteracting Fermi surface corresponding to the actual density obtained by QMC for the specific set of parameters (U, T, μ) [orange contour in Fig. 2(a); see also Fig. 3].

It is also useful to compare with the contour obtained from the momentum distribution function (MDF) [Fig. 4(b)] $n_{\mathbf{k}} = 1/2$ calculated by QMC [shown in white in Fig. 2(a)]. In the thermodynamic limit for a noninteracting system at $T = 0$, the MDF has a jump of size unity $Z = 1$ at the Fermi wave vector $k_F(\mathbf{k})$ when the system transitions from occupied states below k_F to zero occupancy above. In a Fermi liquid, following Luttinger's theorem, $k_F(\mathbf{k})$ does not change upon including electron-electron interactions and $0 < Z \leq 1$. Due to interelectron interactions, some of the states below $k_F(\mathbf{k})$ are scattered into states above but nevertheless in a Fermi liquid, a finite step at k_F persists at $T = 0$. At finite T , naturally the step gets rounded; however, from the peak in the gradient of the MDF [Fig. 4(b)] as a function of \mathbf{k} , we can extract the location of the underlying FS.

From QMC we directly calculate the Green's function in imaginary time τ and from that using an analytic continuation procedure we obtain the spectral function:

$$G_{\mathbf{k}}(\tau) = \int_{-\infty}^{\infty} d\omega \left[\frac{e^{-\omega\tau}}{1 + e^{-\beta\omega}} \right] A_{\mathbf{k}}(\omega). \quad (2)$$

The spectral function $A_{\mathbf{k}}(\omega) = -(1/\pi) \text{Im } G_{\mathbf{k}}^{ret}(\omega)$ gives information about the probability of finding an electron in state (\mathbf{k}, ω) . In the noninteracting and thermodynamic limits the only k states that have spectral weight at $\omega = 0$ are the states on the Fermi surface. For the interacting system, we use this property to find the size of the Fermi surface by examining the k states that are found at zero bias energy.

We implement an iterative maximum-entropy method to calculate the spectral function that most accurately reproduces the input Green's function within error bars [29]. The Fermi surface is constructed by finding the energy that maximizes

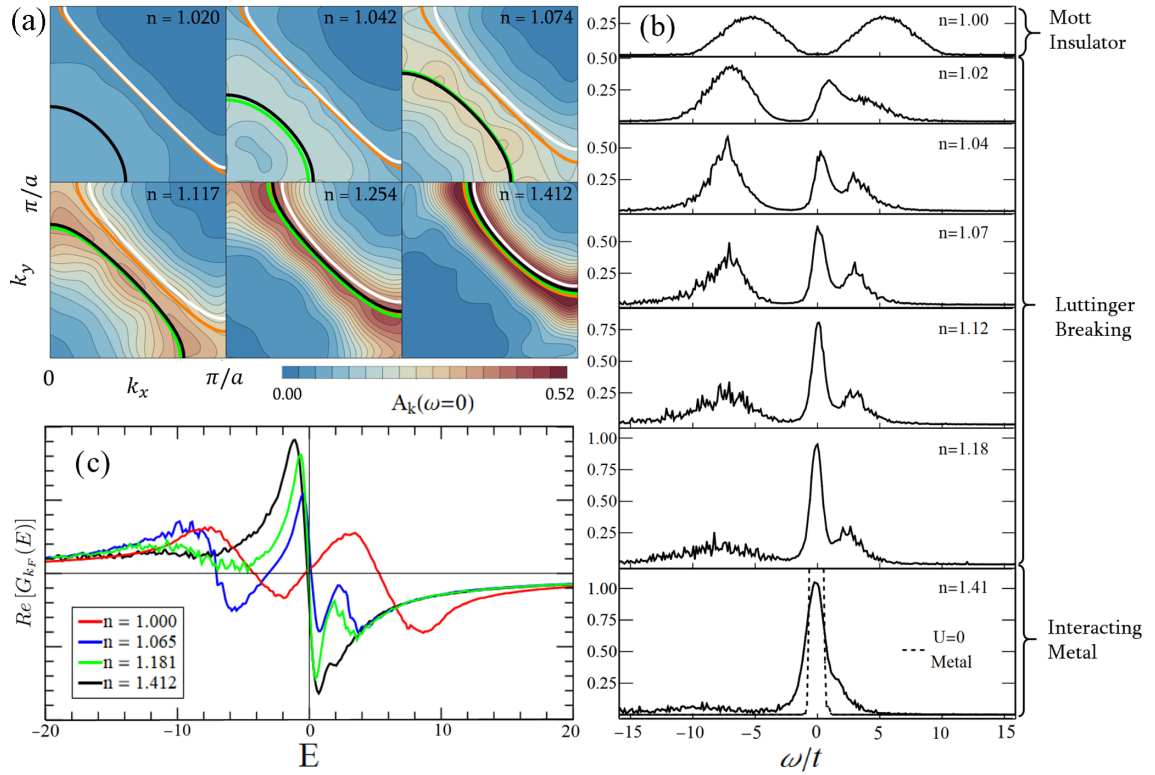


FIG. 2. Spectral functions of Hubbard model: (a) Fermi-surface contours for a square lattice Brillouin zone calculated by 4 different methods for the Hubbard model at $U = 10t$ as a function of density: (i) Luttinger’s theorem applied to a free system (orange); (ii) momentum distribution function (MDF) contour formed by $n_{\mathbf{k}} = 1/2$ (white); (iii) spectral weight at the Fermi energy $A_{\mathbf{k}}(\omega = 0)$ (black); and (iv) the zero of the real part of the retarded Green’s function $G_{\mathbf{k}}^{ret}(E = 0)$ (green). Lattice size 16×16 sites and $\beta t = 2$. (b) Spectral function $A_{\mathbf{k}}(\omega)$ averaged over k states on the Fermi-surface contour. The total spectral weight is normalized $\int_{-\infty}^{\infty} A_{\mathbf{k}}(\omega) d\omega = 1$. For comparison the noninteracting metal spectral function is shown at the same temperature, and on the same lattice size (dashed) and contrasted with the interacting metal for $n = 1.41$. “Interacting metal” is distinguished from the “Luttinger breaking” (LB) regime by the agreement of the MDF and spectral contours. The Mott insulator occurs at $n = 1$. (c) The real part of the Green’s function is calculated using Eq. (4) for the spectral functions shown in (b). A polelike sign change of the Green’s function at $E = 0$ indicates the presence of a quasiparticle on the Fermi surface, consistent with the behavior in a Fermi liquid. The behavior changes dramatically in the Luttinger-breaking regime with sign changes at finite energy. In the Mott insulator at $n = 1$ the Green’s function changes sign at zero energy via a zero, instead of a pole.

the function

$$f(E) = \int_{E=-2t(\cos k_x + \cos k_y)} A_{\mathbf{k}}(\omega = 0) d\mathbf{k}, \quad (3)$$

where E corresponds to a tight-binding contour in the Brillouin zone. In essence, we determine the tight-binding contour that most closely fits the peaks of the spectral function, $A_{\mathbf{k}}(\omega = 0)$ at the energy $E_f = -2t(\cos k_x + \cos k_y)$, thereby locating the approximate Fermi surface. Note that the choice to approximate the Fermi surface with a tight-binding contour [black curve in Fig. 2(a)] is justified by the Hubbard-I approximation (Sec. V).

A related quantity, the real part of the Green’s function, defined by the sum over Matsubara frequencies,

$$\text{Re } G_{\mathbf{k}}(E) = \sum_{\omega_n \neq E} \frac{A_{\mathbf{k}}(\omega_n)}{\omega_n - E} \quad (4)$$

provides a second indicator of the Fermi surface contour as the sign change across $\text{Re } G_{\mathbf{k}}(E = 0)$ marks the Fermi surface boundary (shown in green) [23,34]. We construct the Fermi

surface by finding the contour over the Brillouin zone where the Green’s function changes sign, or when $G_{\mathbf{k}}^{ret}(E = 0) = 0$. When the sign change is polelike, instead of zerolike, a quasiparticle is present on the Fermi surface for momentum \mathbf{k} . Note that while $A_{\mathbf{k}}(\omega = 0)$ uses only information at $\omega = 0$ to map the Fermi-surface contour, $\text{Re } G_{\mathbf{k}}(E = 0)$ uses information over the entire spectral range of $A_{\mathbf{k}}(\omega)$ to map the contour.

IV. RESULTS

For dopings greater than $p \gtrsim 0.2$ each of these methods of finding the FS show stark agreement. Such a validity of Luttinger volume is found even for large U for sufficiently large doping. However, when the doping is less than $p \lesssim 0.2$, we observe a departure of the FS contours obtained from these four methods. The size of the white and orange surfaces, corresponding to the $n_{\mathbf{k}} = 1/2$ contour and the Luttinger surface, respectively, count the total electronic density. The spectral weight and retarded Green’s function boundaries, black and green contours, respectively, on the other hand, recede to include fewer states. In other words, the spectral function

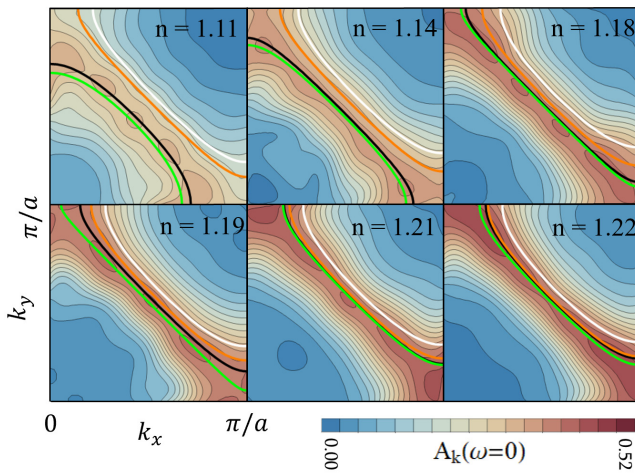


FIG. 3. Fermi-surface contours for a square lattice Brillouin zone calculated by 4 different methods for the Hubbard model at $U = 10t$ as a function of density. (i) Luttinger's theorem applied to a free system (orange); (ii) momentum distribution function (MDF) contour formed by $n_{\mathbf{k}} = 1/2$ (white); (iii) spectral weight at the Fermi energy $A_{\mathbf{k}}(\omega = 0)$ (black); and (iv) singularity of retarded Green's function $G_{\mathbf{k}}^{\text{ret}}(E = 0)$ (green). Lattice size 16×16 sites and $\beta t = 2$.

methods indicate that the Fermi surface is reconfigured from a large Fermi surface enclosing $n = 1 + p$ fermions to a smaller one as quantified in Fig. 1, below a critical density of $n_c \approx 1.2$. As observed in Fig. 2(a), the black and green contours transform from being close to a diamond-shaped Fermi surface to a small circular Fermi surface centered around the Γ point; the deviation occurs for densities $n \lesssim 1.2$. The critical doping at which the FS volume deviates from the Luttinger count is above the doping for the Lifshitz transition at which the FS changes character from holelike to electronlike as the Fermi surface decreases in size, as also seen from Fig. 1, and in agreement with other numerical studies [19]. Our results on the smooth evolution of the FS from obeying the Luttinger

count to a LB Fermi surface are consistent with the measurements of the Hall number in single-layer cuprates such as $\text{Ti}_2\text{Ba}_2\text{CuO}_{6+\delta}$ and $\text{Bi}_2\text{Sr}_2\text{CuO}_{6+\delta}$ [3].

The quasiparticle weight, shown in Fig. 4(a), shows the fraction of the spectral function, $A_{\mathbf{k}_f}(\omega)$, around zero energy, defined by $\text{QW} = \int_{-\epsilon}^{\epsilon} A_{\mathbf{k}_f}(\omega) d\omega$. As a reference we use the $U = 0$ spectral function of the finite-size broadened noninteracting metal from a delta function to a Lorentzian distribution of width 2ϵ in Fig. 2(b) (lowest panel) to account for the resolution in the analytic continuation procedure. The interacting system shows the development of incoherent sidebands or Mott bands around the peaked spectral function at $\omega = 0$. The Fermi-surface restructuring is already visible below $n \approx 1.2$ and the deviation of the actual Fermi contour from the Luttinger contour only gets more pronounced as the incoherent weight increases upon approaching the Mott transition at $n = 1$.

It is important to note that there is no evidence of long-range antiferromagnetic order at the temperatures and parameters at which we are analyzing the Fermi surface. As previously noted [15] the spectral functions obtained by the Hubbard-I approximation [35], which neglects spin correlations, are remarkably similar to the QMC ones at half filling in this range of parameters. The spin structure factor at (π, π) , shown in Fig. 4(c), shows a small peak at $n = 1$ which gets quickly suppressed as the density moves away from this commensurate value. The absence of long-range order in the presence of a reconfiguration of the Fermi surface is a strong indication of some hidden order [25] or topological order in the absence of a Landau symmetry breaking.

V. HUBBARD-I APPROXIMATION

The Luttinger-breaking phase can be qualitatively understood by analyzing the Hubbard-I approximation [15,35], which transforms Eq. (1) via

$$c_{i,\sigma} = c_{i,\sigma} n_{i,-\sigma} + c_{i,\sigma} (1 - n_{i,-\sigma}) \quad (5)$$

$$\equiv (d_{i,\sigma} + h_{i,\sigma}^\dagger). \quad (6)$$

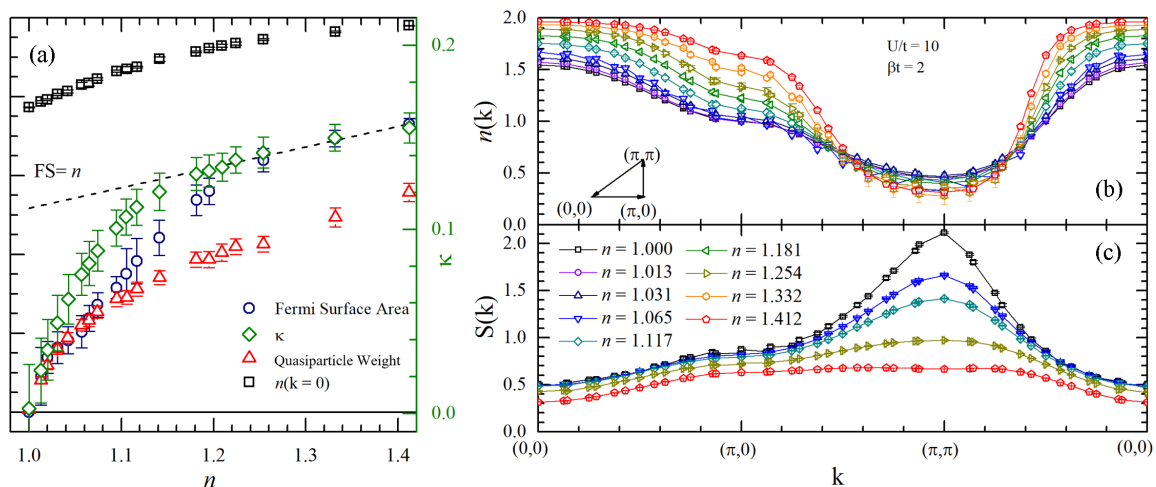


FIG. 4. (a) Behavior of (i) the occupation of the $n_{\mathbf{k}} = (0, 0)$ state, (ii) the quasiparticle weight around the chemical potential, (iii) the compressibility $n^2 \kappa = dn/d\mu$, and (iv) the FS volume (also shown in Fig. 1), all plotted as a function of density. (b) Momentum distribution function $n(\mathbf{k})$ as a function of density for multiple values of n . (c) Structure factor across the Brillouin zone for multiple values of n obtained from the spin-spin correlations showing the absence of long-range magnetic ordering. Lattice size 16×16 , $U = 10t$, $\beta t = 2$.

We have split up the particle annihilation operator into a doublon annihilation and a holon creation operator. The Hamiltonian [Eq. (1)] becomes

$$\begin{aligned} \mathcal{H}_{\text{Hub-I}} = & -\frac{t}{2} \sum_{(i,j),\sigma} (\hat{d}_{i,\sigma}^\dagger \hat{d}_{j,\sigma} + \hat{h}_{i,\sigma} \hat{h}_{j,\sigma}^\dagger) \\ & -\frac{t}{2} \sum_{(i,j),\sigma} (\hat{d}_{i,\sigma}^\dagger \hat{h}_{j,\sigma}^\dagger + \text{H.c.}) - U \sum_{i,\sigma} (\hat{h}_{i,\sigma} \hat{h}_{i,\sigma}^\dagger). \end{aligned} \quad (7)$$

In this picture, the single-particle occupied sites are treated as the background vacuum from which doublons and holons are created and propagate. The Hubbard-I approximation assumes that spin interactions are negligible. We need to account for this by halving the hopping term ($t \rightarrow t/2$) because Pauli exclusion limits the possible avenues for a doublon to hop to a singly occupied site by half. The new operators have anticommutation relations

$$\{\hat{d}_{i,\sigma}, \hat{d}_{j,\sigma'}^\dagger\} = \delta_{i,j}(\delta_{\sigma,\sigma'}(1 - \hat{h}_{i,\sigma}^\dagger \hat{h}_{i,\sigma}) + \delta_{\sigma,-\sigma'} \hat{d}_{i,\sigma} \hat{d}_{j,\sigma'}^\dagger), \quad (8)$$

$$\{\hat{h}_{i,\sigma}, \hat{h}_{j,\sigma'}^\dagger\} = \delta_{i,j}(\delta_{\sigma,\sigma'}(1 - \hat{d}_{i,\sigma}^\dagger \hat{d}_{i,\sigma}) + \delta_{\sigma,-\sigma'} \hat{h}_{i,\sigma} \hat{h}_{j,\sigma'}^\dagger), \quad (9)$$

which we approximate as canonical anti-commutation relations in the limit $U \gg t$ due to the suppression of hopping: $\langle \hat{d}_{i,\sigma}^\dagger \hat{d}_{i,\sigma} \rangle = \langle \hat{h}_{i,\sigma}^\dagger \hat{h}_{i,\sigma} \rangle \approx 0$. The Fourier transform of the Hubbard-I Hamiltonian is

$$\begin{aligned} \mathcal{H}_{\text{Hub-I}} = & \sum_{\mathbf{k},\sigma} \left(\frac{\epsilon_{\mathbf{k}}}{2} \hat{d}_{\mathbf{k},\sigma}^\dagger \hat{d}_{\mathbf{k},\sigma} + \frac{\epsilon_{\mathbf{k}} - U}{2} \hat{h}_{\mathbf{k},\sigma} \hat{h}_{\mathbf{k},\sigma}^\dagger \right) \\ & + \sum_{\mathbf{k},\sigma} \frac{\epsilon_{\mathbf{k}}}{2} (\hat{d}_{\mathbf{k},\sigma}^\dagger \hat{h}_{-\mathbf{k},\sigma}^\dagger + \text{H.c.}) \end{aligned} \quad (10)$$

$$= \Psi_\sigma^\dagger \begin{pmatrix} \frac{\epsilon_{\mathbf{k}}}{2} & \frac{\epsilon_{\mathbf{k}}}{2} \\ \frac{\epsilon_{\mathbf{k}}}{2} & \frac{\epsilon_{\mathbf{k}}}{2} - U \end{pmatrix} \Psi_\sigma, \quad (11)$$

where $\epsilon(\mathbf{k}) = -2t(\cos k_x + \cos k_y)$, and $\Psi_\sigma^\dagger = (\hat{d}_{\mathbf{k},\sigma}^\dagger, \hat{h}_{-\mathbf{k},\sigma})$. Diagonalizing the Bogoliubov-de Gennes Hamiltonian gives the dispersion: two bands each with a bandwidth of approximately t and separated by a gap U ,

$$E^\pm(\mathbf{k}) = \frac{1}{2}(\epsilon(\mathbf{k}) - U \pm \sqrt{\epsilon(\mathbf{k})^2 + U^2}). \quad (12)$$

The associated Brillouin zones for each band possess the same number of states: two spin flavors for every momentum state, which is double the number of degrees of freedom from the traditional Hubbard model, but this is resolved by the redundancy in our implementation: $\hat{d}_{i,\uparrow}^\dagger \hat{d}_{i,\uparrow} = \hat{d}_{i,\downarrow}^\dagger \hat{d}_{i,\downarrow}$, and likewise for holons. The implication of this large- U approximation is that the doped Fermi surface constructed on the Brillouin zone in this limit [Fig. 2(a)] is the Fermi surface of upper-band quasiparticles across the Brillouin zone of upper-band quasiparticles.

The energy bands derived above are explicitly for the half-filled limit. To solve for the energy bands of the doped Hubbard-I model requires analysis of the Green's functions of the doublon and holon operators [36]:

$$E_n^\pm(\mathbf{k}) \approx \frac{1}{2}(\epsilon(\mathbf{k}) - U \pm \sqrt{U^2 + \epsilon(\mathbf{k})^2 - 2(1-n)\epsilon(\mathbf{k})U}). \quad (13)$$

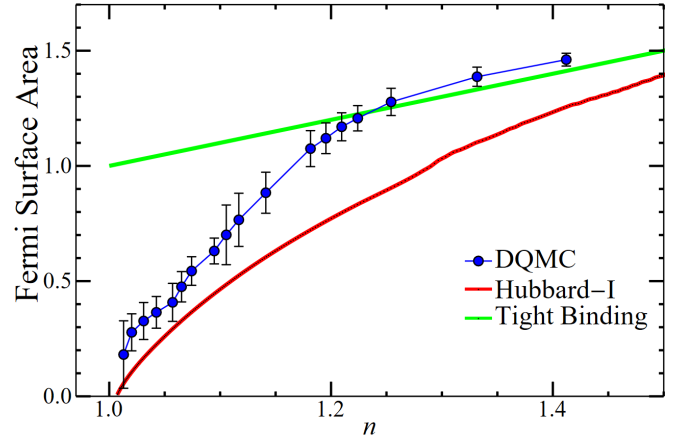


FIG. 5. The Fermi-surface area (FSA) of the well-established Hubbard-I approximation compared to our DQMC results show similar features. The FSA of the doped Hubbard-I model is calculated for the doublon Brillouin zone, and $n = 1 + d$ where d is the doublon density.

The Fermi-surface area is taken to be the number of filled states in the upper band which is a function of $n(\mu)$ and μ . Figure 5 shows the comparison of our results and the Hubbard-I approximation. Attempts to increase the precision of this approximation by adding spin interactions [15] show a similar dependence on the doping at $n \approx 1$.

The compressibility κ serves as a diagnostic of Hubbard-I physics as it is a measure of the number of conducting quasiparticles, which is proportional to the number of states on the Fermi surface. The Mott insulator, where $\kappa(T=0) = 0$, contains no conducting quasiparticles since the chemical potential is in the Hubbard-I band gap. We obtain the compressibility using the fluctuation dissipation theorem:

$$\kappa n^2 = \frac{1}{N_s} \frac{d\langle \hat{N} \rangle}{d\mu} = \frac{\beta}{N_s} (\langle \hat{N}^2 \rangle - \langle \hat{N} \rangle^2), \quad (14)$$

where the number fluctuations $\langle \hat{N}^2 \rangle$ are given in terms of correlation functions $\langle \sum_{i,j} \hat{n}_i \hat{n}_j \rangle$ and calculated directly using QMC techniques.

A Mott insulator to metal transition is driven by tuning the chemical potential at fixed interaction strength, as seen by the strong suppression of the compressibility in Fig. 6(b).

Upon doping the Mott insulator, the system transitions to a strongly interacting metal with suppressed compressibility as shown in Fig. 6(b). The background single-particle occupied sites are frozen and do not contribute to the compressibility, while the excess doubly occupied sites (doublons) are free to propagate.

According to the Hubbard-I approximation, the number of particles on the Fermi surface ($\propto \kappa$) in the tight-binding model for an electron density n is about twice that of the number of quasiparticles on the Fermi surface in the upper Hubbard-I band for an electron density $n/2 + 1$, which we verify is qualitatively correct in Fig. 6(c).

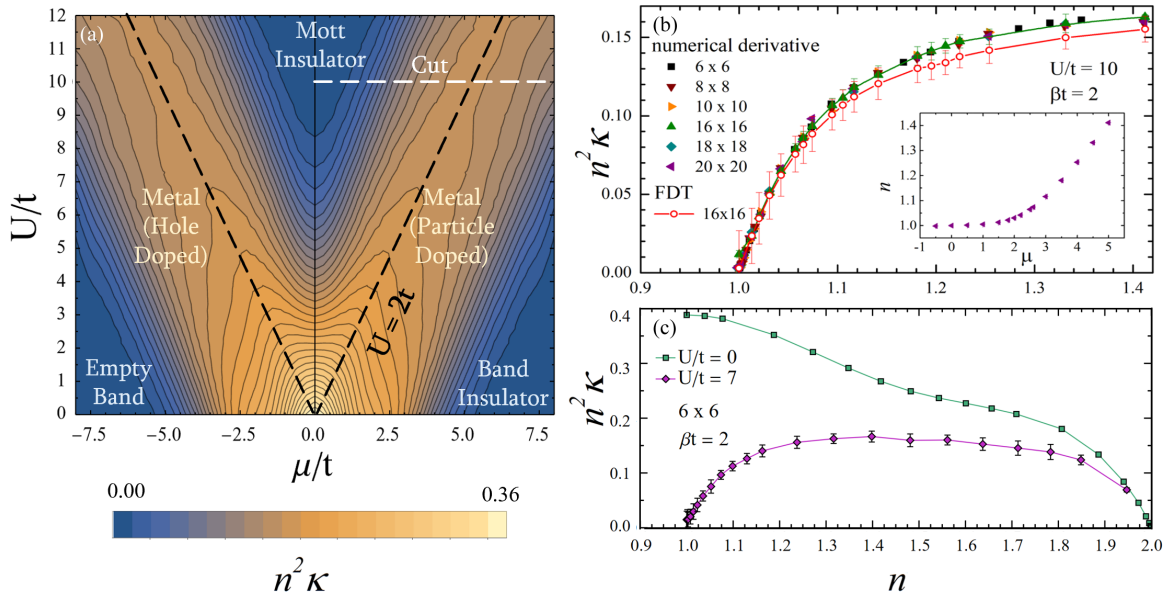


FIG. 6. (a) Compressibility, κn^2 , is calculated on a 6×6 lattice as a function of interaction potential (U) and chemical potential (μ) at $\beta t = 2$. The compressibility is a measure of the number of conducting quasiparticles which is proportional to the number of particles on the Fermi surface. (b) Compressibility is examined for lattice sizes from 6×6 to 16×16 with a fixed interaction strength ($U = 10t$) and varying density/chemical potential (μ) for $\beta t = 2$. Closed symbols are data extracted from numerical derivatives $dn/d\mu$ and open symbols from fluctuation dissipation theorem. (c) Compressibility of a strongly interacting system and a noninteracting system shows distinct evidence for Hubbard-I physics.

VI. LOWER TEMPERATURES

Does the Luttinger-breaking phase survive to lower temperatures? The Hubbard-I approximation implies that we should see this effect at zero temperature. In Fig. 7 we show the Fermi surface for $n = 1.03$ and $n = 1.07$, as well as for the temperatures $\beta = 2$ and $\beta = 3/t$. We find that the LB phase is present at both densities and survives to lower temperatures.

Our results are explained by the fractionalization of the spectral function which can only increase at lower temperatures. Furthermore, it is striking that even at temperatures as high as $\beta = 2/t$ one is able to see the LB phase. While lower temperatures do need to be examined to get a more refined picture of this phase, the presence of the LB phase above and below the exchange temperature of $T = 4t^2/U$ is a clear sign that it is not arising from magnetic ordering.

VII. DISCUSSION AND OUTLOOK

We have presented QMC simulation results coupled with analytic continuation to obtain spectral functions of the Hubbard model in two dimensions. We have obtained the Fermi-surface contour by analyzing the spectral function at the chemical potential μ . As the system approaches half filling, most of the spectral weight resides in a broad incoherent lump.

With increase in electron or hole density, we see sharp spectral features at μ but the volume enclosed by the zero-energy contour at μ falls short of the Luttinger count and does not enclose all the electrons. This ‘‘Luttinger breaking’’ (LB) region in density is consistent with the strange metal region discussed in cuprates [3] and persists to about 18% in our simulations. Our results suggest that if secondary ordering in the

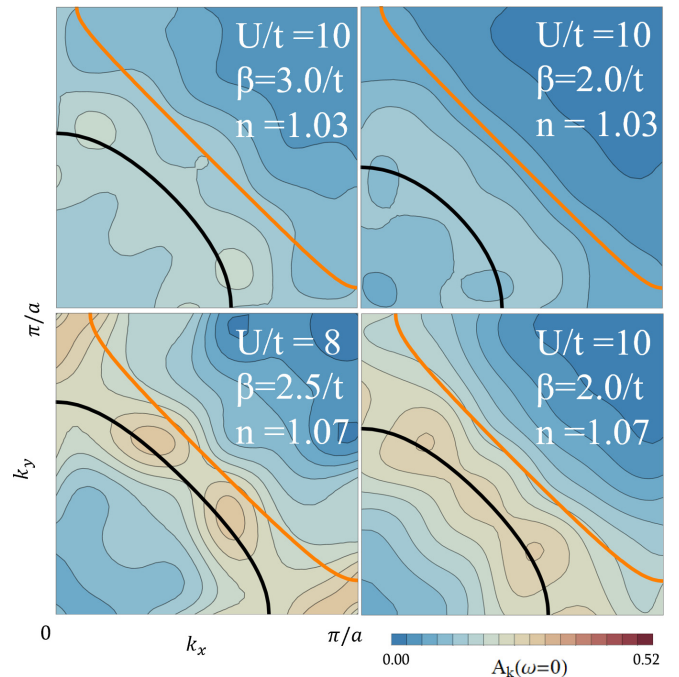


FIG. 7. On the left, we show the function $A_{\mathbf{k}}(\omega = 0)$ plotted over the reduced Brillouin zone for smaller temperatures than examined in the bulk of this paper. Compare these figures with their equal-density, high- T counterparts found on the right. The black curve is the maximal noninteracting contour of the function $A_{\mathbf{k}}(\omega = 0)$ and the orange contour is the noninteracting Fermi surface that obeys Luttinger’s theorem. The bottom left figure is simulated at smaller U/t ; however, the phenomenon of the Luttinger-breaking phase persists. We note that the effect persists at temperatures lower than the critical exchange temperature of $\beta = U/4t^2$.

spin, charge, or pairing channel is suppressed, the proximity to a Mott insulator alone drives the formation of such a LB phase.

A topological framework [23,37,38] for understanding the transition from a Fermi liquid obeying the Luttinger count to the LB phase that violates this count is obtained by expressing the Luttinger volume as the winding number of the single-particle Green's function at finite temperatures. Further, the winding number can be connected with the distribution of quasiparticles and the Luttinger volume, and it can be shown nonperturbatively that for a strongly interacting Hamiltonian that preserves particle-hole symmetry both types of behavior, pole and zero, of the Green's function at zero energy are observed.

It has been suggested that doped quantum spin liquids are perhaps a promising platform observing non-Fermi-liquid phases. Sachdev, Senthil, and collaborators have proposed the possibility of a non-Fermi-liquid phase (dubbed FL*) with a Fermi surface composed of fractionalized spinons with a volume $(n-1) \bmod 2$ [39]. They claim that quantum fluctuations of the antiferromagnetic order parameter generate emergent gauge fields that lead to a new state of matter with topological order [40–42]. Further diagnostics on the entanglement properties of these non-Fermi-liquid phases are required to understand the connection between our discovery of the LB phase that encloses a shrinking volume below a critical density as the Mott insulator is approached and the proposed FL* phases that encloses a Luttinger volume of $(n-1)$.

Going forward, further simulations are necessary to study an extended Hubbard model with nearest-neighbor hopping to describe the more realistic parameters for the cuprates. Here our aim was to show the emergence of the Luttinger-breaking phase in the very simplest case with only nearest-neighbor hopping. It would also be interesting to push the calculations to lower temperatures to see the emergence of the superconducting phase from the LB phase and contrast that with the superconducting phase that emerges from the FL phase above this critical value.

ACKNOWLEDGMENTS

We acknowledge useful discussions with Hasan Khan during the initial stages of this project. We also acknowledge insightful discussions with Mohit Randeria, Aavishkar Patel, Philip Philips, and Sumilan Banerjee. I.O. and N.T. acknowledge the support of the DOE-BES Grant No. DE-FG02-07ER46423. T.P. acknowledges support from CNPq, FAPERJ, and Instituto Nacional de Ciência e Tecnologia de Informação Quântica (INCT-IQ).

APPENDIX: SOURCES OF ERROR

We discuss below sources of errors in the determinantal QMC (DQMC) simulations and in the maximum-entropy procedure to extract the spectral function.

1. Finite-size effects

We have obtained data for different system sizes, ranging from 6×6 to 20×20 . Figure 6(b) clearly shows that finite-size effects are smaller than error bars for the compressibility for

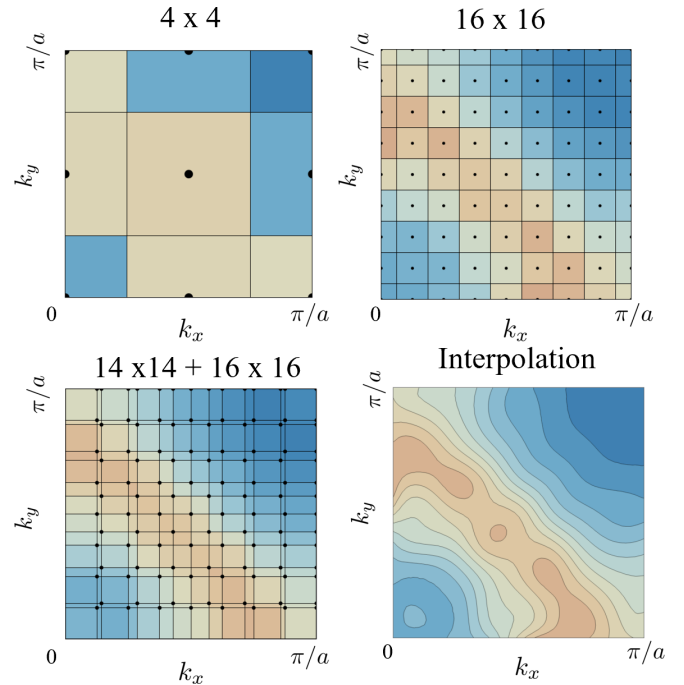


FIG. 8. The effect of cluster size on the resolution of the Brillouin zone and efforts to improve resolution.

$\beta t = 2$ and $U/t = 10$. Finite-size effects in transport data from quantum Monte Carlo simulations were shown to be most relevant for particular densities with closed-shell configurations and small U/t [43], not the cases considered here.

In Fig. 8 we show the locations of the k points for different size lattices and it becomes quickly evident that a finer mesh is essential to see the structure of the spectral functions near the Fermi surface.

We use a technique of combining multiple complimentary cluster sizes to increase the number of unique momentum states from which we can resolve features of the Brillouin zone. The technique works best for system sizes where $L_1/2$ shares no common factors with $L_2/2$, where L^2 is the number of lattice sites. Instead of overlapping, one Brillouin zone fills in the gaps of the other and the resolution increases. We do not change any other parameters except system size and check that the size does not have a significant effect on any thermodynamic properties. We combine data from $L_1 = 16$ and $L_2 = 14$. A demonstration of the effect of combining data has on the resolution is shown in Fig. 8. Lastly, we use a spline interpolation function to construct $A(k, \omega = 0)$ as a function for all k in the Brillouin zone in the thermodynamic limit.

2. Trotter errors

We calculate thermodynamic properties and the single-particle Green's function by implementing a determinantal QMC algorithm which essentially employs a Trotter-Suzuki decomposition to break up the noncommuting hopping and interaction terms in imaginary time τ [44–47]. This maps the original 2D quantum problem to a $(2+1)$ D classical problem where the extra dimension is set by the inverse temperature $\beta = 1/(k_B T)$. In the quantum Monte Carlo implementation used here the interaction term is decoupled through a

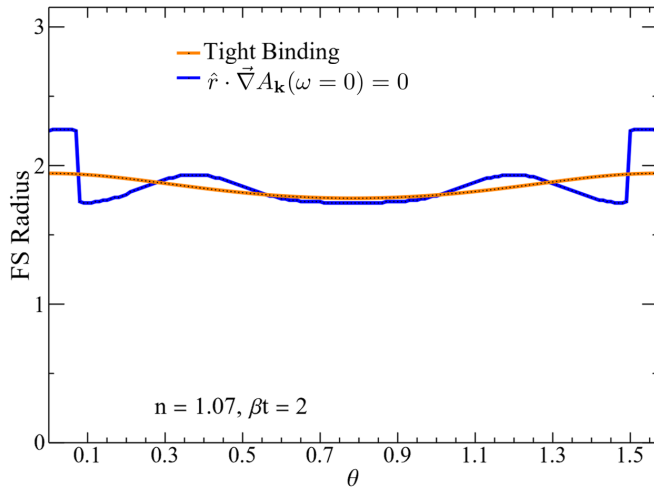


FIG. 9. Blue: The maximum of the function $A_{\mathbf{k}}(\omega = 0)$ for $n = 1.07$ along a contour defined by a straight line that starts at the Gamma point of the Brillouin zone and makes an angle θ with the k_x axis. Orange: The noninteracting Fermi surface (FS) that closely tracks with the interacting Fermi surface. The fluctuations in the interacting Fermi surface are taken to be spurious and due to both finite-size effects and error in the maximum-entropy procedure.

discrete Hubbard-Stratonovich transformation, which introduces an auxiliary Ising field [46] that leads to an error $\mathcal{O}(\Delta\tau^2)$. Extrapolations to $\Delta\tau^2 \rightarrow 0$ show that the coefficient of $\Delta\tau^2$ changes in value and sign for different quantities [43], but for $\Delta\tau = 1/40$ used here the error should be negligible.

3. Maximum-entropy procedure

The calculation of the spectral function $A_{\mathbf{k}}(\omega)$ is done by numerically performing the inverse Laplace transformation in Eq. (7) at a given temperature. There are different available procedures to perform the analytical continuation in the literature [28,30,32,33] but our purpose here is not to perform a systematic study of the different methods' outstanding issues; instead, we adopt the maximum-entropy procedure [29].

The use of tight-binding contours to approximate the Fermi surface is justified based on the Hubbard-I approximation and error in the maximum-entropy procedure. Figure 9 compares the maximum of the function $A_{\mathbf{k}}(\omega = 0)$ for $n = 1.07$ along radial lines starting from the Gamma point and making an angle θ with the k_x axis, and the tight-binding contour which maximizes the function $f(E)$ in Eq. (3). We present the noninteracting contour in figures like Fig. 2(a) and Fig. 3 because it encloses approximately the same number of states as the interacting contour, which has fluctuations due to errors in the maximum-entropy procedure and finite-size effects. We choose not to allow the spurious fluctuations to become a focus.

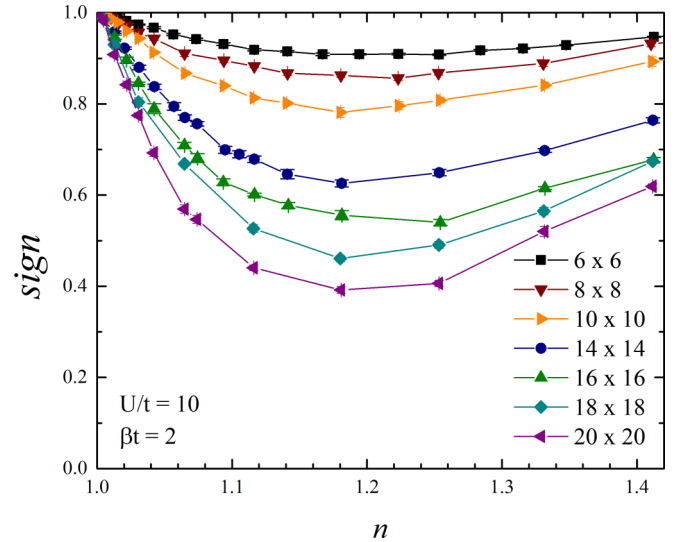


FIG. 10. Average total sign as a function of density for lattice sizes from 6×6 to 20×20 . Temperature is set such that $\beta t = 2$, and the interaction potential is $U = 10t$.

4. Sign problem

In DQMC the grand partition function is expressed as a sum over all Ising spin configurations $c \equiv \{s\}$ at each space-time lattice point, of a product of determinants,

$$\mathcal{Z} = \left(\frac{1}{2}\right)^{L^d M} \text{Tr}_{\{s\}} \det O^\uparrow(\{s\}) \cdot \det O^\downarrow(\{s\}), \quad (\text{A1})$$

where $M = \beta/\Delta\tau$, L is the linear size of the system, and d the dimension. The ‘‘Boltzmann weight’’ is given by the product $p(c) = \det O^\uparrow(\{s\}) \cdot \det O^\downarrow(\{s\})$ which is not always positive. We can keep track of the sign by writing

$$p(c) = \text{sign}(c)|p(c)|, \quad (\text{A2})$$

where $\text{sign}(c) = \pm 1$; this way the absolute value is used as the weight in the Monte Carlo procedure and the sign is included in the measurements. Any expectation value $\langle A \rangle$ is then given by

$$\langle A \rangle = \frac{\sum_c p(c)A(c)}{\sum_c p(c)} = \frac{\sum_c |p(c)|\text{sign}(c)A(c)}{\sum_c |p(c)|\text{sign}(c)} \equiv \frac{\langle \text{sign}A \rangle}{\langle \text{sign} \rangle}. \quad (\text{A3})$$

At low temperatures, both $\langle \text{sign}A \rangle$ and $\langle \text{sign} \rangle$ become very small, leading to the well known ‘‘fermion sign problem.’’ [45,48,49]. The fermion sign problem is also known to get worse with increasing system size as is shown in Fig. 10. We have then restricted our system sizes to lattices up to 16×16 , where $\langle \text{sign} \rangle > 0.5$.

[1] J. M. Luttinger, *Phys. Rev.* **119**, 1153 (1960).
 [2] S. Badoux, W. Tabis, F. Lalibert e, G. Grissonnache, B. Vignolle, D. Vignolles, J. B eard, D. A. Bonn, W. N. Hardy, R. Liang, N. Doiron-Leyraud, L. Taillefer, and C. Proust, *Nature (London)* **531**, 210214 (2016).

[3] C. Putzke, S. Benhabib, W. Tabis, J. Ayres, Z. Wang, L. Malone, S. Licciardello, J. Lu, T. Kondo, T. Takeuchi, N. E. Hussey, J. R. Cooper, and A. Carrington, *Nat. Phys.* **17**, 826 (2021).
 [4] J. E. Hoffman, E. W. Hudson, K. M. Lang, V. Madhavan, H. Eisaki, S. Uchida, and J. C. Davis, *Science* **295**, 466 (2002).

- [5] T. Hanaguri, C. Lupien, Y. Kohsaka, D. Lee, M. Azuma, M. Takano, H. Takagi, and J. Davis, *Nature (London)* **430**, 1001 (2004).
- [6] W. Wise, M. Boyer, K. Chatterjee, T. Kondo, T. Takeuchi, H. Ikuta, Y. Wang, and E. Hudson, *Nat. Phys.* **4**, 696 (2008).
- [7] H. Ding, M. R. Norman, T. Yokoya, T. Takeuchi, M. Randeria, J. C. Campuzano, T. Takahashi, T. Mochiku, and K. Kadowaki, *Phys. Rev. Lett.* **78**, 2628 (1997).
- [8] J. C. Campuzano, M. Norman, and M. Randeria, *The Physics of Superconductors, Vol. II: Superconductivity in Nanostructures, High- T_c and Novel Superconductors, Organic Superconductors*, edited by K.-H. Bennemann and J. B. Ketterson (Springer, 2002), pp. 167–273.
- [9] A. Loeser, Z. Shen, D. Dessau, D. Marshall, C. Park, P. Fournier, and A. Kapitulnik, *Science* **273**, 325329 (1996).
- [10] M. R. Norman, H. Ding, M. Randeria, J. C. Campuzano, T. Yokoya, T. Takeuchi, T. Takahashi, T. Mochiku, K. Kadowaki, P. Guptasarma, and D. G. Hinks, *Nature (London)* **392**, 157160 (1998).
- [11] A. P. Mackenzie, S. R. Julian, D. C. Sinclair, and C. T. Lin, *Phys. Rev. B* **53**, 5848 (1996).
- [12] N. Bulut, D. J. Scalapino, and S. R. White, *Phys. Rev. B* **50**, 7215(R) (1994).
- [13] R. Preuss, W. Hanke, and W. von der Linden, *Phys. Rev. Lett.* **75**, 1344 (1995).
- [14] A. Moreo, S. Haas, A. W. Sandvik, and E. Dagotto, *Phys. Rev. B* **51**, 12045 (1995).
- [15] C. Gröber, R. Eder, and W. Hanke, *Phys. Rev. B* **62**, 4336 (2000).
- [16] S. Sakai, Y. Motome, and M. Imada, *Phys. Rev. Lett.* **102**, 056404 (2009).
- [17] M. Civelli, M. Capone, S. S. Kancharla, O. Parcollet, and G. Kotliar, *Phys. Rev. Lett.* **95**, 106402 (2005).
- [18] E. Gull, M. Ferrero, O. Parcollet, A. Georges, and A. J. Millis, *Phys. Rev. B* **82**, 155101 (2010).
- [19] K.-S. Chen, Z. Y. Meng, T. Pruschke, J. Moreno, and M. Jarrell, *Phys. Rev. B* **86**, 165136 (2012).
- [20] K.-S. Chen, S. Pathak, S.-X. Yang, S.-Q. Su, D. Galanakis, K. Mikelsons, M. Jarrell, and J. Moreno, *Phys. Rev. B* **84**, 245107 (2011).
- [21] H. Bragança, S. Sakai, M. C. O. Aguiar, and M. Civelli, *Phys. Rev. Lett.* **120**, 067002 (2018).
- [22] B. S. Shastry, *Ann. Phys.* **405**, 155 (2019).
- [23] I. Dzyaloshinskii, *Phys. Rev. B* **68**, 085113 (2003).
- [24] T. D. Stanescu and G. Kotliar, *Phys. Rev. B* **74**, 125110 (2006).
- [25] L. Taillefer, *Annu. Rev. Condens. Matter Phys.* **1**, 51 (2010).
- [26] Y. Kakehashi and P. Fulde, *Phys. Rev. Lett.* **94**, 156401 (2005).
- [27] T. A. Maier, T. Pruschke, and M. Jarrell, *Phys. Rev. B* **66**, 075102 (2002).
- [28] J. E. Gubernatis, M. Jarrell, R. N. Silver, and D. S. Sivia, *Phys. Rev. B* **44**, 6011 (1991).
- [29] A. W. Sandvik, *Phys. Rev. B* **57**, 10287 (1998).
- [30] M. Jarrell and J. E. Gubernatis, *Phys. Rep.* **269**, 133 (1996).
- [31] K. Bouadim, Y. L. Loh, M. Randeria, and N. Trivedi, *Nat. Phys.* **7**, 884889 (2011).
- [32] R. Levy, J. LeBlanc, and E. Gull, *Comput. Phys. Commun.* **215**, 216403 (2017).
- [33] A. W. Sandvik, *Phys. Rev. E* **94**, 063308 (2016).
- [34] K. B. Dave, P. W. Phillips, and C. L. Kane, *Phys. Rev. Lett.* **110**, 090403 (2013).
- [35] J. Hubbard, *Proc. R. Soc. London A* **276**, 238 (1963).
- [36] E. Pavarini, E. Koch, R. Scalettar, and R. Martin, eds., *The Physics of Correlated Insulators, Metals, and Superconductors*, Schriften des Forschungszentrums Jülich, Reihe Modeling and Simulation (Forschungszentrum Jülich GmbH Zentralbibliothek, Verlag, Jülich, 2017), Vol. 7, p. 450 S.
- [37] M. Oshikawa, *Phys. Rev. Lett.* **84**, 3370 (2000).
- [38] K. Seki and S. Yunoki, *Phys. Rev. B* **96**, 085124 (2017).
- [39] T. Senthil, S. Sachdev, and M. Vojta, *Phys. Rev. Lett.* **90**, 216403 (2003).
- [40] M. S. Scheurer, S. Chatterjee, W. Wu, M. Ferrero, A. Georges, and S. Sachdev, *Proc. Natl. Acad. Sci. USA* **115**, E3665 (2018).
- [41] W. Wu, M. S. Scheurer, S. Chatterjee, S. Sachdev, A. Georges, and M. Ferrero, *Phys. Rev. X* **8**, 021048 (2018).
- [42] D. G. Joshi, C. Li, G. Tarnopolsky, A. Georges, and S. Sachdev, *Phys. Rev. X* **10**, 021033 (2020).
- [43] R. Mondaini, K. Bouadim, T. Paiva, and R. R. dos Santos, *Phys. Rev. B* **85**, 125127 (2012).
- [44] R. Blankenbecler, D. J. Scalapino, and R. L. Sugar, *Phys. Rev. D* **24**, 2278 (1981).
- [45] R. R. dos Santos, *Braz. J. Phys.* **33**, 36 (2003).
- [46] J. E. Hirsch, *Phys. Rev. B* **28**, 4059 (1983).
- [47] J. E. Hirsch, *Phys. Rev. B* **31**, 4403 (1985).
- [48] E. Y. Loh, J. E. Gubernatis, R. T. Scalettar, S. R. White, D. J. Scalapino, and R. L. Sugar, *Phys. Rev. B* **41**, 9301 (1990).
- [49] V. I. Iglovikov, E. Khatami, and R. T. Scalettar, *Phys. Rev. B* **92**, 045110 (2015).